

# Radiative decay of $^{229m}\text{Th}$ in solid-state nuclear clocks

Zong-Heng Li(李宗珩) and Xu Wang(王旭)<sup>†</sup>

Graduate School, China Academy of Engineering Physics, Beijing 100193, China

(Received 27 October 2025; revised manuscript received 7 January 2026; accepted manuscript online 28 January 2026)

The  $^{229}\text{Th}$  isotope hosts an exceptionally low-energy nuclear transition in the vacuum ultraviolet range, making it a leading candidate for nuclear optical clocks. Recent laser excitation and fluorescence measurements in Th-doped crystals have demonstrated the feasibility of such clocks, yet the precise lifetime of the nuclear excited state remains uncertain. In this work, we build upon the well-established  $n^3$  scaling of  $M1$  nuclear decay rates, which describes how the radiative decay of a magnetic-dipole transition is modified by the refractive index  $n$  of an isotropic and homogeneous medium. Our contribution unifies previously disparate experimental results on  $^{229}\text{Th}$ -doped crystals within a single theoretical framework and delineates the conditions under which the scaling remains valid. We further analyze the limitations of extracting vacuum lifetimes from existing solid-state measurements, highlighting the roles of non-radiative decay channels as well as surface and defect-induced effects, which can invalidate the simple  $n^3$  rule under realistic experimental conditions. These insights open new possibilities for reducing interrogation times and improving the overall performance of nuclear clocks.

**Keywords:** nuclear optical clock, thorium-229, quantum optics in dielectric**PACS:** 42.50.-p, 76.80.+y, 33.45.+x**DOI:** 10.1088/1674-1056/ae3e72**CSTR:** 32038.14.CPB.ae3e72

## 1. Introduction

The  $^{229}\text{Th}$  isotope features a low-energy isomeric state ( $^{229m}\text{Th}$ ) approximately 8.4 eV above the nuclear ground state,<sup>[1–9]</sup> making it the only known nuclear level directly accessible to vacuum ultraviolet (VUV) laser excitation.<sup>[10–12]</sup> This unique property positions  $^{229m}\text{Th}$  as a prime candidate for nuclear optical clocks,<sup>[13–16]</sup> which promise unprecedented precision in timekeeping and offer novel avenues for testing fundamental physics.<sup>[17–19]</sup> A leading platform is the solid-state nuclear clock, which embeds  $^{229}\text{Th}$  nuclei into wide-band-gap crystals that are transparent to the VUV nuclear transition. This approach offers distinct advantages, including ultrahigh nuclear density and suppression of recoil and first-order Doppler effects, making it highly competitive with — and potentially superior to — current atomic optical clocks.<sup>[14–16,20,21]</sup>

Substantial progress over the past two decades has steadily revealed the properties of  $^{229m}\text{Th}$ . The first direct observation of its radiative decay was achieved at CERN,<sup>[22]</sup> where  $^{229}\text{Ac}$  nuclei were implanted into  $\text{CaF}_2$  and  $\text{MgF}_2$  crystals, subsequently producing  $^{229m}\text{Th}$  via  $\beta$  decay. This experiment resulted in a transition frequency uncertainty at the terahertz level and determined a radiative half-life of 670(102) s. More recently, RIKEN reported a half-life of  $1400^{+600}_{-300}$  s by trapping  $^{229m}\text{Th}^{3+}$  ions from a  $^{233}\text{U}$  source in an ion trap.<sup>[23]</sup>

The first resonant excitation of  $^{229m}\text{Th}$  was reported by a PTB group,<sup>[24]</sup> using a  $\text{Th}:\text{CaF}_2$  crystal with a high concen-

tration of  $^{229}\text{Th}$  provided by TU Wien,<sup>[21]</sup> which was irradiated by a pulsed VUV laser source generated via four-wave mixing.<sup>[11]</sup> A subsequent direct laser excitation was reported by a UCLA group,<sup>[25]</sup> using a  $^{229}\text{Th}$ -doped  $\text{LiSrAlF}_6$  crystal and a similar pulsed VUV laser source.<sup>[10]</sup> These studies reported fluorescence lifetimes (note that lifetime=half-life/ $\ln 2$ ) in the Th-doped  $\text{CaF}_2$  and  $\text{LiSrAlF}_6$  crystals of 630(15) s and 568(13)<sub>stat</sub>(20)<sub>sys</sub> s, respectively. More recently, a JILA group demonstrated direct excitation of the narrow nuclear clock transition in a  $\text{Th}:\text{CaF}_2$  crystal using a single line from a VUV frequency comb, yielding a lifetime of 641(4) s.<sup>[26]</sup> Additionally, a group from Okayama University used x-rays to pump  $^{229}\text{Th}$  nuclei in a  $\text{Th}:\text{CaF}_2$  crystal to the second excited state at 29 keV,<sup>[27]</sup> which partially decayed into  $^{229m}\text{Th}$ , reporting a radiative lifetime of 645(36) s.

Unlike the fixed radiative lifetime in vacuum, the radiative decay in dielectric crystals is modified by the altered photon density of states.<sup>[28,29]</sup> We believe it is timely and valuable for the nuclear-clock community to present a detailed theoretical framework describing the radiative lifetime of  $^{229m}\text{Th}$  in dielectric environments and to assess the current progress in this area. In this work, we develop such a framework for the radiative decay of  $^{229m}\text{Th}$  in solid-state nuclear clocks. By canonically quantizing the spatial electromagnetic modes and incorporating local-field effects, we provide a comprehensive description of the radiative decay dynamics. We specify when the  $M1$   $n^3$  scaling is valid — particularly for an isotropic and homogeneous medium. We also point out the possible uncer-

<sup>†</sup>Corresponding author. E-mail: [xwang@gascaep.ac.cn](mailto:xwang@gascaep.ac.cn)

tainties arising from factors such as non-radiative decay channels and proximity to interfaces, which complicate the direct application of the  $n^3$  scaling to experimental data. Our results elucidate how the crystal environment reshapes nuclear radiative processes, offering insights for optimizing fluorescence detection and enhancing the performance of solid-state nuclear clocks.

## 2. Radiative decay rate of $^{229m}\text{Th}$ in vacuum

We first consider the radiative decay of a  $^{229m}\text{Th}$  nucleus in vacuum. The Hamiltonian of the vacuum radiation field is given by

$$\begin{aligned} H_{\text{rad}} &= \frac{1}{2} \int \left[ \epsilon_0 \mathbf{E}^2(\mathbf{r}) + \frac{1}{\mu_0} \mathbf{B}^2(\mathbf{r}) \right] d^3r \\ &= \frac{\hbar}{2} \int d\mathbf{k} \sum_{\mu} \omega_{\mathbf{k}} (a_{\mathbf{k},\mu}^{\dagger} a_{\mathbf{k},\mu} + \text{h.c.}), \end{aligned} \quad (1)$$

where  $\epsilon_0$  and  $\mu_0$  are the vacuum permittivity and permeability, respectively.  $\hbar$  is the reduced Planck constant,  $\omega_{\mathbf{k}} = c|\mathbf{k}|$  with  $c$  being the speed of light in vacuum, and  $a_{\mathbf{k},\mu}$  is the annihilation operator of electromagnetic mode  $(\mathbf{k}, \mu)$ . The electric and magnetic field operators are quantized to become

$$\begin{aligned} \mathbf{E}(\mathbf{r}) &= \int d\mathbf{k} \sum_{\mu} i \sqrt{\frac{\hbar \omega_{\mathbf{k}}}{2\epsilon_0 (2\pi)^3}} a_{\mathbf{k},\mu} \mathbf{e}_{\mu}(\mathbf{k}) e^{i\mathbf{k}\cdot\mathbf{r}} + \text{h.c.}, \\ \mathbf{B}(\mathbf{r}) &= \int d\mathbf{k} \sum_{\mu} i \sqrt{\frac{\hbar \omega_{\mathbf{k}}}{2\epsilon_0 (2\pi)^3}} \frac{1}{c} a_{\mathbf{k},\mu} \mathbf{e}'_{\mu}(\mathbf{k}) e^{i\mathbf{k}\cdot\mathbf{r}} + \text{h.c.}, \end{aligned} \quad (2)$$

where  $\mathbf{e}_{\mu}(\mathbf{k})$  is the unit polarization vector, and

$$\mathbf{e}'_{\mu}(\mathbf{k}) = \mathbf{e}_{\mu}(\mathbf{k}) \times \mathbf{k}/k.$$

Using the Coulomb gauge, the vector potential of the electromagnetic field is given by

$$\mathbf{A}(\mathbf{r}) = \int d\mathbf{k} \sum_{\mu} \sqrt{\frac{\hbar}{2\omega_{\mathbf{k}}\epsilon_0(2\pi)^3}} a_{\mathbf{k},\mu} \mathbf{e}_{\mu}(\mathbf{k}) e^{i\mathbf{k}\cdot\mathbf{r}} + \text{h.c.} \quad (3)$$

The unit vector potential of the electromagnetic wave mode  $(\mathbf{k}, \mu)$  can be expanded in a multipole series as

$$\begin{aligned} \mathbf{A}_{\mu}(\mathbf{k}, \mathbf{r}) &= \mathbf{e}_{\mu}(\mathbf{k}) e^{i\mathbf{k}\cdot\mathbf{r}} \\ &= 4\pi \sum_{lm} i^l [(e_{\mu}(\mathbf{k}) \cdot \mathbf{Y}_{lm,l}^*(\mathbf{k})) \mathbf{A}_{lm}(k, \mathbf{r}, M) \\ &\quad + (e'_{\mu}(\mathbf{k}) \cdot \mathbf{Y}_{lm,l}^*(\mathbf{k})) \mathbf{A}_{lm}(k, \mathbf{r}, E)], \end{aligned} \quad (4)$$

where the vector spherical harmonics  $\mathbf{Y}_{lm,l}$  are defined in Ref. [30].  $\mathbf{A}_{lm}(\mathbf{k}, \mathbf{r}, \tau)$  are transverse vector spherical harmonics, given by

$$\begin{aligned} \mathbf{A}_{lm}(k, \mathbf{r}, M) &= \frac{1}{\sqrt{l(l+1)}} \mathbf{L} [j_l(kr) \mathbf{Y}_{lm}(\mathbf{r})], \\ \mathbf{A}_{lm}(k, \mathbf{r}, E) &= \frac{-i}{k\sqrt{l(l+1)}} \nabla \times \mathbf{L} [j_l(kr) \mathbf{Y}_{lm}(\mathbf{r})], \end{aligned} \quad (5)$$

where  $j_l(kr)$  is the Bessel function of the first kind and  $\mathbf{Y}_{lm}$  are the spherical harmonics. These two transverse vector spherical harmonics correspond to magnetic and electric multipole transitions, respectively.

The interaction Hamiltonian between the vacuum radiation field and the nucleus is given by

$$H_{\text{int}} = - \int \mathbf{j}(\mathbf{r}) \cdot \mathbf{A}(\mathbf{r}) d^3r, \quad (6)$$

where  $\mathbf{j}$  is the nuclear current density operator. For a nuclear transition with frequency  $\omega_0$ , it is convenient to introduce the multipole transition operators and the reduced transition probability for radiative transitions of multipole order  $\tau l$ :

$$\begin{aligned} \mathcal{M}(Ml, m) &= \frac{-i(2l+1)!!}{k_0^l c(l+1)} \int \mathbf{j}(\mathbf{r}) \cdot \mathbf{L} [j_l(k_0 r) \mathbf{Y}_{lm}(\mathbf{r})] d^3r, \\ \mathcal{M}(El, m) &= \frac{(2l+1)!!}{k_0^{l+1} c(l+1)} \int \mathbf{j}(\mathbf{r}) \cdot \nabla \times \mathbf{L} [j_l(k_0 r) \mathbf{Y}_{lm}(\mathbf{r})] d^3r, \\ B(\tau l) &= \frac{1}{2I_e + 1} |\langle I_g \| \mathcal{M}(\tau l) \| I_e \rangle|^2, \quad \tau = M, E, \end{aligned} \quad (7)$$

where  $k_0 = \omega_0/c$  is the wave number corresponding to the transition frequency.

Assuming that the initial and final states of the combined nucleus-field system are

$$|i\rangle = |I_e M_e\rangle |0\rangle, \quad |f\rangle = |I_g M_g\rangle |1_{\mathbf{k},\mu}\rangle,$$

where  $I_{e,g}$  and  $M_{e,g}$  are the spin and magnetic quantum numbers of the nuclear states,  $|0\rangle$  is the vacuum state of the radiation field, and  $|1_{\mathbf{k},\mu}\rangle$  denotes a single photon state with mode  $(\mathbf{k}, \mu)$ . The transition rate between the initial and the final states is given by Fermi's golden rule:

$$\begin{aligned} w &= \frac{2\pi}{\hbar^2} \int d\mathbf{k} \sum_{\mu} |\langle f | H_{\text{int}} | i \rangle|^2 \delta(\omega_{\mathbf{k}} - \omega_0) \\ &= \frac{2\pi}{\hbar^2} \int d\mathbf{k} \sum_{\mu} \frac{\hbar}{2\omega_{\mathbf{k}}\epsilon_0(2\pi)^3} |\langle I_g M_g | -\mathbf{j}(\mathbf{r}) \cdot \mathbf{A}(\mathbf{r}) | I_e M_e \rangle|^2 \delta(\omega_{\mathbf{k}} - \omega_0) \\ &= \sum_{lm} \sum_{\tau=E,M} \frac{2k_0^{2l+1}}{\hbar\epsilon_0} \frac{l+1}{l[(2l+1)!!]^2} |\langle I_g M_g | \mathcal{M}(\tau l, m) | I_e M_e \rangle|^2. \end{aligned} \quad (8)$$

After averaging over initial states, summing over final states, and using the Wigner–Eckart theorem, we obtain the nuclear decay rate in vacuum:

$$\begin{aligned}\Gamma &= \frac{1}{2I_e + 1} \sum_{M_g} w = \sum_l \sum_{\tau=E,M} \frac{2k_0^{2l+1}}{\hbar\epsilon_0} \frac{l+1}{l[(2l+1)!!]^2} B(\tau l) \\ &\equiv \sum_l \sum_{\tau=E,M} \Gamma^{\tau l},\end{aligned}\quad (9)$$

where  $\Gamma^{\tau l}$  is the nuclear decay rate of multipole order  $\tau l$  in vacuum.

$$\begin{aligned}H_{\text{rad}}^n &= \frac{1}{2} \int \left[ \epsilon_r \epsilon_0 \mathfrak{E}^2(\mathbf{r}) + \frac{1}{\mu_r \mu_0} \mathfrak{B}^2(\mathbf{r}) \right] d^3r = \frac{\hbar}{2} \int d\mathbf{K} \sum_{\mu} \omega_{\mathbf{K}} (b_{\mathbf{K},\mu}^{\dagger} b_{\mathbf{K},\mu} + \text{h.c.}), \\ \mathfrak{E}(\mathbf{r}) &= \int d\mathbf{K} \sum_{\mu} i \sqrt{\frac{\hbar \omega_{\mathbf{K}}}{2\epsilon_r \epsilon_0 (2\pi)^3}} b_{\mathbf{K},\mu} e_{\mu}(\mathbf{K}) e^{i\mathbf{K}\cdot\mathbf{r}} + \text{h.c.}, \\ \mathfrak{B}(\mathbf{r}) &= \int d\mathbf{K} \sum_{\mu} i \sqrt{\frac{\hbar \omega_{\mathbf{K}} \mu_r}{2\epsilon_0 (2\pi)^3}} \frac{1}{c} b_{\mathbf{K},\mu} e'_{\mu}(\mathbf{K}) e^{i\mathbf{K}\cdot\mathbf{r}} + \text{h.c.}, \\ \mathfrak{A}(\mathbf{r}) &= \int d\mathbf{K} \sum_{\mu} \sqrt{\frac{\hbar}{2\omega_{\mathbf{K}} \epsilon_r \epsilon_0 (2\pi)^3}} b_{\mathbf{K},\mu} e_{\mu}(\mathbf{K}) e^{i\mathbf{K}\cdot\mathbf{r}} + \text{h.c.},\end{aligned}\quad (10)$$

where  $\epsilon_r$  and  $\mu_r$  are the relative permittivity and permeability of the medium with  $\epsilon_r \mu_r = n^2$ .  $\omega_{\mathbf{K}} = c\mathbf{K}/n$  and  $b_{\mathbf{K},\mu}$  are the annihilation operators of electromagnetic mode  $(\mathbf{K}, \mu)$ .

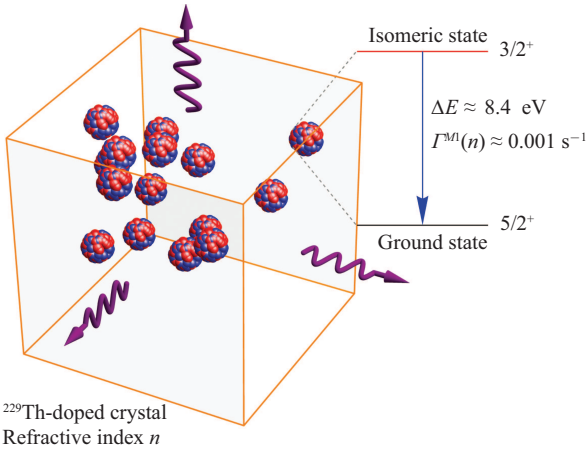


**Fig. 1.** Schematic illustration of  $^{229}\text{Th}$ -doped crystal with refractive index  $n$ . The transition energy between the ground state and the isomeric state inside the crystal is approximately 8.4 eV. The measured lifetime ( $1/e$  decay time) of  $^{229m}\text{Th}$  is about  $10^2$ – $10^3$  s, corresponding to a decay rate of about  $0.001 \text{ s}^{-1}$ .

The interaction Hamiltonian between the radiation field and the nucleus is given by

$$H_{\text{int}}^n = - \int \mathbf{j}(\mathbf{r}) \cdot \mathfrak{A}(\mathbf{r}) d^3r. \quad (11)$$

Using Fermi's golden rule, averaging over initial states and summing over final states, we obtain the modified nuclear decay rate in the continuous medium:

$$\Gamma_n = \frac{1}{2I_e + 1} \sum_{M_g} \frac{2\pi}{\hbar^2} \int d\mathbf{K} \sum_{\mu} |\langle f | H_{\text{int}}^n | i \rangle|^2 \delta(\omega_{\mathbf{K}} - \omega_0)$$

### 3. Radiative decay rate of $^{229m}\text{Th}$ in continuous medium

We now consider a space filled with a transparent, homogeneous, and isotropic medium with a refractive index  $n$  and a band gap that exceeds the nuclear transition energy. The  $^{229}\text{Th}$  nuclei are doped into this medium, which is, in fact, a bulk crystal. A schematic illustration of this system is shown in Fig. 1. We then proceed to introduce the Hamiltonian of the radiation field within the medium, along with the corresponding quantized field operator

$$\begin{aligned}&= \sum_l \sum_{\tau=E,M} \frac{2k_0^{2l+1}}{\hbar\epsilon_0} \frac{l+1}{l[(2l+1)!!]^2} B(\tau l) \times \eta_r^{\tau l} \\ &\equiv \sum_l \sum_{\tau=E,M} \Gamma^{\tau l} \times \eta_r^{\tau l},\end{aligned}\quad (12)$$

where  $\eta_r^{\tau l}$  is the enhancement factor for the nuclear transition of multipole order  $\tau l$ , given by

$$\begin{aligned}\eta_r^{Ml} &= \frac{n^{2l+3}}{\epsilon_r} = n^{2l+1} \mu_r, \\ \eta_r^{El} &= \frac{n^{2l+1}}{\epsilon_r}.\end{aligned}\quad (13)$$

We emphasize that the above results apply only to homogeneous and isotropic media that are transparent to 148-nm VUV radiation. Real crystals may exhibit defects, anisotropy, and other material-specific complexities, whose effects lie beyond the scope of the present work.

### 4. Local field effect

In the previous derivation, we performed a macroscopic quantization of the radiation field in a continuous medium. However, from a purely microscopic perspective, the medium is not perfectly continuous, and an empty space, or ‘‘cavity,’’ exists around the emitter inside the dielectric. As a result, the local field acting on the emitter does not directly correspond to the macroscopic radiation field derived from a continuous medium. A similar issue arises in the derivation of the Clausius–Mossotti law.<sup>[31]</sup> To account for this local field effect, one assumes that the size of the cavity is large compared to the dimension of the emitter but small compared to

the involved wavelength. The material outside the cavity is treated as a homogeneous dielectric. However, different models for such a cavity yield varying results.<sup>[32]</sup> Specifically, the value of the local field at the position of the emitter depends on whether the cavity is modeled as a real (Onsager model<sup>[28]</sup>) or a virtual (Lorentz model<sup>[33]</sup>) cavity.

In the real-cavity model, the electromagnetic fields inside and outside the cavity are related by a boundary condition derived from Maxwell's equations. Inside the cavity, the emitter is surrounded by vacuum. Outside the cavity, the space is filled with a continuous medium with refractive index  $n$ . Classical electrodynamics shows that the electric field in this cavity is enhanced by a factor of  $3\epsilon_r/(1+2\epsilon_r)$ ,<sup>[28]</sup> regardless of the cavity size. The virtual-cavity model assumes no physical vacuum cavity; instead, it accounts for the polarization of the surrounding medium induced by the emitter. According to the derivation of the Clausius–Mossotti law, the electric field felt by the emitter is enhanced by a factor of  $(\epsilon_r+2)/3$ . The real-cavity model is more appropriate for situations in which interactions between the surrounding atoms or molecules are weak, whereas the virtual-cavity model is applicable when the electric fields produced by polarized atoms or molecules significantly influence their surroundings.<sup>[31]</sup>

For the dielectric materials commonly used in solid-state nuclear clocks (*e.g.*,  $\text{CaF}_2$ ,  $\text{MgF}_2$ ), the magnetic susceptibility equals the vacuum value ( $\mu_r = 1$ ); therefore, we have  $\epsilon_r = n^2$ . Based on the models above, the local electric field strength acting on the emitter is corrected by the factor:

$$\eta_{\text{loc}}^E = \begin{cases} \frac{3n^2}{2n^2+1}, & \text{for the real-cavity model,} \\ \frac{n^2+2}{3}, & \text{for the virtual-cavity model.} \end{cases} \quad (14)$$

Correspondingly, the magnetic field acting on the emitter is not corrected by the local field effect, leading to a factor  $\eta_{\text{loc}}^M = 1$ .

The final modified radiative decay rate for a nuclear transition of multipole order  $\tau l$  is given by

$$\begin{aligned} \Gamma^{\tau l}(n) &= \Gamma^{\tau l} \times \eta_r^{\tau l} \times (\eta_{\text{loc}}^{\tau})^2 \\ &\equiv \Gamma^{\tau l} \times \eta^{\tau l}. \end{aligned} \quad (15)$$

The factor  $\eta^{\tau l}$  ( $\tau = E$  or  $M$ ) between the radiative decay rate in the medium and that in the vacuum is given by

$$\eta^{Ml} = n^{2l+1},$$

$$\eta^{El} = \begin{cases} \frac{9n^{2l+3}}{(2n^2+1)^2}, & \text{for the real-cavity model,} \\ n^{2l-1} \left( \frac{n^2+2}{3} \right)^2, & \text{for the virtual-cavity model.} \end{cases} \quad (16)$$

## 5. Current experimental results and discussion

This section summarizes the current experimental results of the radiative decay rates of  $^{229\text{m}}\text{Th}$  in various dielectric crystals. The ground state of the  $^{229}\text{Th}$  nucleus has spin-parity

$5/2^+$ , and the isomeric state has spin-parity  $3/2^+$ . Consequently, the primary transition type is magnetic dipole ( $M1$ ), with electric quadrupole ( $E2$ ) transitions serving as secondary channels. The nuclear transition matrix elements are quantified by the reduced transition probabilities  $B(\tau l)$ . Recent experimental analyses of the  $M1$  transition have yielded values consistent to the same order of magnitude.<sup>[22–24,26,27]</sup> Although  $M1$  and  $E2$  transitions coexist, the  $M1$  decay rate significantly exceeds that of the  $E2$  transition, which is typically the case for transition energies below 1 MeV.<sup>[30]</sup> Therefore, the radiative decay lifetime associated with the  $E2$  transition is substantially longer than that of the  $M1$  transition in  $^{229\text{m}}\text{Th}$ . Experimental measurements indicate that the typical vacuum lifetime of  $^{229\text{m}}\text{Th}$  is approximately  $10^3$  seconds, rendering the  $E2$  decay signals undetectable under standard experimental conditions, and the  $B(E2)$  value is usually derived from theoretical models. The decay of the  $^{229\text{m}}\text{Th}$  nucleus can be effectively modeled as an  $M1$  transition.

The authors in Ref. [23] reported the only direct measurement of the isomer lifetime in vacuum using an ion trap, yielding a half-life of  $1400_{-300}^{+600}$  s (or a lifetime of  $2020_{-433}^{+865}$  s). Here we adopt the following values for the reduced nuclear transition probabilities<sup>[23,34]</sup>:

$$\begin{aligned} B(M1) &= 0.0272 \text{ W.u.}, \\ B(E2) &= 42.9 \text{ W.u.}, \end{aligned} \quad (17)$$

where W.u. denotes Weisskopf units. These values correspond to vacuum radiative lifetimes of approximately 2020 seconds for the  $M1$  transition and about  $2 \times 10^5$  years for the  $E2$  transition. Even after accounting for local-field-induced enhancements of the  $E2$  decay rate ( $10^{-13} \text{ s}^{-1} \sim 10^{-12} \text{ s}^{-1}$  for the two local-field models considered), the nuclear transition of  $^{229\text{m}}\text{Th}$  can be unambiguously identified as an  $M1$  transition, with a decay rate of order  $\sim 10^{-3} \text{ s}^{-1}$  in currently studied solid-state hosts.

Compared to the radiative decay in vacuum, the  $M1$  decay rate in a crystal with refractive index  $n$  is accelerated by a factor of  $\eta^{M1}(n) = n^3$ , and the observed lifetimes from the fluorescence spectra should be corrected accordingly. Table 1 and Fig. 2 summarize the observed lifetimes of  $^{229\text{m}}\text{Th}$  from recent experiments and the corresponding inferred vacuum lifetimes. It is evident that the inferred vacuum lifetimes exhibit significant discrepancies between experiments. Several factors contribute to these variations.

(i)  $\text{Th}:\text{CaF}_2$  experiments: These experiments utilized crystals provided by the same group at TU Wien<sup>[21]</sup> and reported close results, corresponding to a vacuum isomer lifetime of about 2500 s.

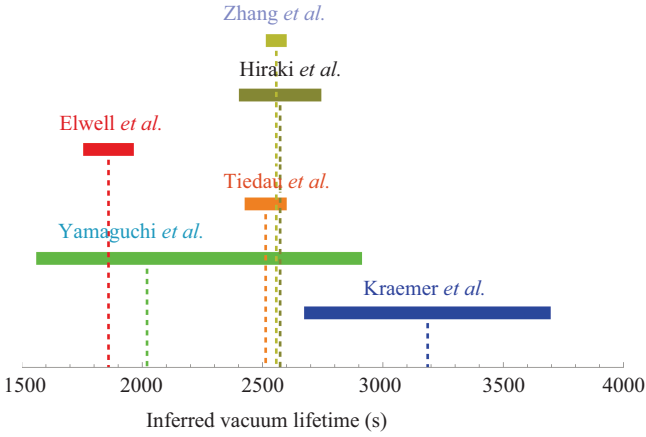


**Fig. 2.** The comparisons of the inferred vacuum lifetime of  $^{229m}\text{Th}$ . The measurement results are arranged in chronological order from bottom to top. Dashed lines indicate the central values inferred from each experiment, while the bar charts represent the associated uncertainties.

(ii)  $\text{Th}:\text{MgF}_2$  experiments: In this experiment,  $^{229}\text{Fr}$  and  $^{229}\text{Ra}$  ion beams were implanted into  $\text{MgF}_2$  crystals at 30 keV, subsequently decaying to  $^{229m}\text{Th}$  via the  $\beta$ -decay chain. The shallow implantation depth (approximately tens of nanometers) raises concerns about the applicability of the

$n^3$ -dependence in this context, which is valid only for a bulk dielectric. Further investigations with more precise lifetime measurements and varied implantation conditions are necessary to validate the observed decay rates.

(iii)  $\text{Th}:\text{LiSrAlF}_6$  experiments: The observed fluorescence lifetime in this crystal is notably shorter than in other experiments (such as  $\text{Th}:\text{CaF}_2$ ). This discrepancy may be attributed to an underestimation of the crystal's refractive index, as the refractive index of  $\text{LiSrAlF}_6$  has not been well characterized.<sup>[25]</sup> Potential non-radiative decay channels may also accelerate the isomer decay in  $\text{Th}:\text{LiSrAlF}_6$ . As discussed in Ref. [37], doping  $^{229}\text{Th}$  into crystals can generate spatially localized electronic defect states with energies lower than the nuclear transition frequency, thereby enabling internal conversion (IC) channels. Density functional theory (DFT) calculations support the existence of such defect states in  $\text{Th}:\text{LiSrAlF}_6$ . By contrast, a recent CASPT2 study reports defect-state energies of approximately 11 eV in  $\text{Th}:\text{CaF}_2$ ,<sup>[38]</sup> which precludes IC channels in that host.

**Table 1.** Radiative lifetime of  $^{229m}\text{Th}$  obtained from experiments.

Doped crystal	Refractive index $n$	Observed lifetime (s)	Inferred vacuum lifetime (s)
$\text{MgF}_2$	1.488 <sup>[22]</sup>	967(147) <sup>[22]</sup>	3186(484)
$\text{CaF}_2$	1.586 <sup>[24,35,36]</sup>	630(15) <sup>[24]</sup>	2513(60)
		641(4) <sup>[26]</sup>	2557(16)
		645(36) <sup>[27]</sup>	2573(144)
$\text{LiSrAlF}_6$	1.485 <sup>[25]</sup>	568(13) <sub>stat</sub> (20) <sub>sys</sub> <sup>[25]</sup>	1860(78)
None	1 <sup>[23]</sup>	2020 <sup>+865</sup> <sub>-433</sub> <sup>a</sup>	2020 <sup>+865</sup> <sub>-433</sub>

<sup>a</sup>Ref. [23]: Measurement with trapped ions instead of doped crystals.

Assuming the observed fluorescence lifetime in  $\text{Th}:\text{CaF}_2$  results solely from radiative decay, a vacuum decay rate of  $4.0 \times 10^{-4} \text{ s}^{-1}$  can be derived. Applying this value to  $\text{Th}:\text{LiSrAlF}_6$  (where  $n = 1.488$ ) yields a predicted radiative decay rate of  $1.3 \times 10^{-3} \text{ s}^{-1}$ , which is notably lower than the experimental value of  $1.8 \times 10^{-3} \text{ s}^{-1}$ . This discrepancy could be attributed to a non-radiative decay rate of about  $4.8 \times 10^{-4} \text{ s}^{-1}$ . Nevertheless, typical IC decay rates are on the order of  $10^3 \text{ s}^{-1}$ , several orders of magnitude faster than the rate calculated here. Further investigation of non-radiative decay mechanisms is therefore warranted to assess the extent to which such channels contribute in  $\text{Th}:\text{LiSrAlF}_6$ .

## 6. Conclusion

In this study, we developed a theoretical framework for the radiative decay of the  $^{229m}\text{Th}$  nuclear isomer in Th-doped dielectric crystals. By applying macroscopic quantization to the radiation field within these materials, we demonstrate that

the  $M1$  decay rate is enhanced by a factor of  $n^3$ , where  $n$  is the refractive index of the host crystal. This enhancement significantly influences the observed fluorescence lifetimes, necessitating corrections to account for the medium's refractive properties.

Recent experimental results reveal notable discrepancies in the derived vacuum isomer lifetimes across different crystal hosts. These variations underscore the interplay between the crystal environment and nuclear decay processes and provide critical insights into the design and potential optimization of solid-state nuclear clocks. Future research should focus on refining the characterization of crystal properties to enhance the coherence and stability of nuclear transitions in these materials.

## Appendix A:

The Hamiltonian of the electromagnetic field in the vacuum can be obtained from the following formulas:

$$\begin{aligned}
 \int d^3r \varepsilon_0 \mathbf{E}^2(\mathbf{r}) &= \int d^3r \varepsilon_0 \iint d\mathbf{k}_1 d\mathbf{k}_2 \sum_{\mu_1 \mu_2} \left( i \sqrt{\frac{\hbar \omega_{\mathbf{k}_1}}{2\varepsilon_0 (2\pi)^3}} a_{\mathbf{k}_1, \mu_1} e_{\mu_1}(\mathbf{k}_1) e^{i\mathbf{k}_1 \cdot \mathbf{r}} + \text{h.c.} \right) \\
 &\quad \times \left( i \sqrt{\frac{\hbar \omega_{\mathbf{k}_2}}{2\varepsilon_0 (2\pi)^3}} a_{\mathbf{k}_2, \mu_2} e_{\mu_2}(\mathbf{k}_2) e^{i\mathbf{k}_2 \cdot \mathbf{r}} + \text{h.c.} \right) \\
 &= \frac{\hbar}{2(2\pi)^3} \iint d\mathbf{k}_1 d\mathbf{k}_2 \sum_{\mu_1 \mu_2} e_{\mu_1}(\mathbf{k}_1) \cdot e_{\mu_2}(\mathbf{k}_2) \sqrt{\omega_{\mathbf{k}_1} \omega_{\mathbf{k}_2}} \int d^3r \left( a_{\mathbf{k}_1, \mu_1} a_{\mathbf{k}_2, \mu_2}^\dagger e^{i(\mathbf{k}_1 - \mathbf{k}_2) \cdot \mathbf{r}} + \text{h.c.} \right) \\
 &= \frac{\hbar}{2} \int d\mathbf{k} \sum_{\mu} \omega_{\mathbf{k}} \left( a_{\mathbf{k}, \mu} a_{\mathbf{k}, \mu}^\dagger + \text{h.c.} \right), \\
 \int d^3r \frac{1}{\mu_0} \mathbf{B}^2(\mathbf{r}) &= \int d^3r \frac{1}{\mu_0} \iint d\mathbf{k}_1 d\mathbf{k}_2 \sum_{\mu_1 \mu_2} \left( i \sqrt{\frac{\hbar \omega_{\mathbf{k}_1}}{2\varepsilon_0 (2\pi)^3}} \frac{1}{c} a_{\mathbf{k}_1, \mu_1} e'_{\mu_1}(\mathbf{k}_1) e^{i\mathbf{k}_1 \cdot \mathbf{r}} + \text{h.c.} \right) \\
 &\quad \times \left( i \sqrt{\frac{\hbar \omega_{\mathbf{k}_2}}{2\varepsilon_0 (2\pi)^3}} \frac{1}{c} a_{\mathbf{k}_2, \mu_2} e'_{\mu_2}(\mathbf{k}_2) e^{i\mathbf{k}_2 \cdot \mathbf{r}} + \text{h.c.} \right) \\
 &= \frac{\hbar}{2(2\pi)^3} \iint d\mathbf{k}_1 d\mathbf{k}_2 \sum_{\mu_1 \mu_2} e'_{\mu_1}(\mathbf{k}_1) \cdot e'_{\mu_2}(\mathbf{k}_2) \sqrt{\omega_{\mathbf{k}_1} \omega_{\mathbf{k}_2}} \int d^3r \left( a_{\mathbf{k}_1, \mu_1} a_{\mathbf{k}_2, \mu_2}^\dagger e^{i(\mathbf{k}_1 - \mathbf{k}_2) \cdot \mathbf{r}} + \text{h.c.} \right) \\
 &= \frac{\hbar}{2} \int d\mathbf{k} \sum_{\mu} \omega_{\mathbf{k}} \left( a_{\mathbf{k}, \mu} a_{\mathbf{k}, \mu}^\dagger + \text{h.c.} \right). \tag{A1}
 \end{aligned}$$

For a continuous medium one simply makes the following substitution:  $\varepsilon_0 \rightarrow \varepsilon_0 \varepsilon_r$  and  $\mu_0 \rightarrow \mu_0 \mu_r$ .

The annihilation and creation operators in vacuum satisfy the following commutation relations:

$$\begin{aligned}
 [a_{\mathbf{k}_1, \mu_1}, a_{\mathbf{k}_2, \mu_2}] &= 0, \\
 [a_{\mathbf{k}_1, \mu_1}^\dagger, a_{\mathbf{k}_2, \mu_2}^\dagger] &= 0, \\
 [a_{\mathbf{k}_1, \mu_1}, a_{\mathbf{k}_2, \mu_2}^\dagger] &= \delta(\mathbf{k}_1 - \mathbf{k}_2) \delta_{\mu_1, \mu_2}. \tag{A2}
 \end{aligned}$$

The operators  $b_{\mathbf{K}, \mu}, b_{\mathbf{K}, \mu}^\dagger$  in a continuous medium satisfy the commutation relations above as well.

In vacuum and in continuous media, the photon density of states per unit volume in the range between  $\omega$  and  $\omega + d\omega$  is

$$\begin{aligned}
 \rho(\omega_{\mathbf{k}}) &= 2 \frac{1}{(2\pi)^3} \frac{\int_{\Omega_{\mathbf{k}}} d\mathbf{k}}{d\omega_{\mathbf{k}}} = \frac{\omega_{\mathbf{k}}^2}{\pi^2 c^3}, \\
 \rho(\omega_{\mathbf{K}}) &= 2 \frac{1}{(2\pi)^3} \frac{\int_{\Omega_{\mathbf{K}}} d\mathbf{K}}{d\omega_{\mathbf{K}}} = n^3 \frac{\omega_{\mathbf{K}}^2}{\pi^2 c^3}. \tag{A3}
 \end{aligned}$$

Here we use  $\omega_{\mathbf{k}} = ck$  and  $\omega_{\mathbf{K}} = cK/n$ .

## Acknowledgment

Project supported by the National Natural Science Foundation of China (Grant Nos. 12474484, U2330401, and 12088101).

## References

- [1] Kroger L A and Reich C W 1976 *Nucl. Phys. A* **259** 29
- [2] Reich C W and Helmer R G 1990 *Phys. Rev. Lett.* **64** 271
- [3] Helmer R G and Reich C W 1994 *Phys. Rev. C* **49** 1845

- [4] Beck B R, Becker J A, Beiersdorfer P, Brown G V, Moody K J, Wilhelmly J B, Porter F S, Kilbourne C A and Kelley R L 2007 *Phys. Rev. Lett.* **98** 142501
- [5] von der Wense L, Seiferle B, Laatiaoui M, Neumayr J B, Maier H J, Wirth H F, Mokry C, Runke J, Eberhardt K, Düllmann C E, Trautmann N G and Thierolf P G 2016 *Nature* **533** 47
- [6] Thielking J, Okhapkin M V, Glowacki P, Meier D M, von der Wense L, Seiferle B, Düllmann C E, Thierolf P G and Peik E 2018 *Nature* **556** 321
- [7] Seiferle B, von der Wense L, Bilous P V, Amersdorffer I, Lemell C, Libisch F, Stellmer S, Schumm T, Düllmann C E, Pálffy A and Thierolf P G 2019 *Nature* **573** 243
- [8] Yamaguchi A, Muramatsu H, Hayashi T, Yuasa N, Nakamura K, Takimoto M, Haba H, Konashi K, Watanabe M, Kikunaga H, Maehata K, Yamasaki N Y and Mitsuda K 2019 *Phys. Rev. Lett.* **123** 222501
- [9] Sikorsky T, Geist J, Hengstler D, Kempf S, Gastaldo L, Enss C, Mokry C, Runke J, Düllmann C E, Wobrowschek P, Beeks K, Rosecker V, Sterba J H, Kazakov G, Schumm T and Fleischmann A 2020 *Phys. Rev. Lett.* **125** 142503
- [10] Jeet J 2018 *Search for the low lying transition in the  $^{229}\text{Th}$  nucleus*, Ph.D. Dissertation (Los Angeles: University of California, Los Angeles)
- [11] Zhang C, Li P, Jiang J, von der Wense L, Doyle J F, Fermann M E and Ye J 2022 *Opt. Lett.* **47** 5591
- [12] Thielking J, Zhang K, Tiedau J, Zander J, Zitzer G, Okhapkin M V and Peik E 2023 *New J. Phys.* **25** 083026
- [13] Peik E and Tamm C 2003 *Europhys. Lett.* **61** 181
- [14] Rellergert W G, DeMille D, Greco R R, Hehnen M P, Torgerson J R and Hudson E R 2010 *Phys. Rev. Lett.* **104** 200802
- [15] Campbell C J, Radnaev A G, Kuzmich A, Dzuba V A, Flambaum V V and Derevianko A 2012 *Phys. Rev. Lett.* **108** 120802
- [16] Kazakov G A, Litvinov A N, *et al.* 2012 *New J. Phys.* **14** 083019
- [17] Flambaum V V 2006 *Phys. Rev. Lett.* **97** 092502
- [18] Berengut J C, Dzuba V A, Flambaum V V and Porsev S G 2009 *Phys. Rev. Lett.* **102** 210801
- [19] Fadeev P, Berengut J C and Flambaum V V 2020 *Phys. Rev. A* **102** 052833
- [20] Stellmer S, Schreitl M and Schumm T 2015 *Sci. Rep.* **5** 15580
- [21] Beeks K, Sikorsky T, Rosecker V, Pressler M, Schaden F, Werban D, Hosseini N, Rudischer L, Schneider F, Berwian P, Friedrich J, Hainz D, Welch J, Sterba J H, Kazakov G and Schumm T 2023 *Sci. Rep.* **13** 3897
- [22] Kraemer S, Moens J, Athanasakis-Kaklamanakis M, *et al.* 2023 *Nature* **617** 706

- [23] Yamaguchi A, Shigekawa Y, Haba H, Kikunaga H, Shirasaki K, Wada M and Katori H 2024 *Nature* **629** 62
- [24] Tiedau J, Okhapkin M V, Zhang K, Thielking J, Zitzer G, Peik E, Schaden F, Pronebner T, Morawetz I, Toscani De Col L, Schneider F, Leitner A, Pressler M, Kazakov G A, Beeks K, Sikorsky T and Schumm T 2024 *Phys. Rev. Lett.* **132** 182501
- [25] Elwell R, Schneider C, Jeet J, Terhune J E S, Morgan H W T, Alexandrova A N, Tran Tan H B, Derevianko A and Hudson E R 2024 *Phys. Rev. Lett.* **133** 013201
- [26] Zhang C, Ooi T, Higgins J S, Doyle J F, von der Wense L, Beeks K, Leitner A, Kazakov G A, Li P, Thirolf P G, Schumm T and Ye J 2024 *Nature* **633** 63
- [27] Hiraki T, Okai K, Bartokos M, *et al.* 2024 *Nat. Commun.* **15** 5536
- [28] Glauber R J and Lewenstein M 1991 *Phys. Rev. A* **43** 467
- [29] Tkalya E V 2000 *JETP Lett.* **71** 311
- [30] Greiner W and Maruhn J A 1996 *Nuclear Models* (Berlin: Springer Berlin, Heidelberg) pp. 75–98
- [31] von Hippel A R 1995 *Dielectrics and Waves* (London: Artech House) pp. 97–98 and 178–181
- [32] Rikken G L J A and Kessener Y A R R 1995 *Phys. Rev. Lett.* **74** 880
- [33] Crenshaw M E and Bowden C M 2000 *Phys. Rev. Lett.* **85** 1851
- [34] Minkov N and Pálffy A 2021 *Phys. Rev. C* **103** 014313
- [35] Daimon M and Masumura A 2002 *Appl. Opt.* **41** 5275
- [36] Zheng Q, Wang X and Thompson D 2023 *Opt. Mater. Express* **13** 2380
- [37] Morgan H W T, Tran Tan H B, Elwell R, Alexandrova A N, Hudson E R and Derevianko A 2025 *Phys. Rev. Lett.* **134** 253801
- [38] Nalikowski K, Veryazov V, Beeks K, Schumm T and Kro’snicki M 2025 *Phys. Rev. B* **111** 115103